Astron. Astrophys. 148, 217–225 (1985)

ASTRONOMY AND ASTROPHYSICS

# Acoustic waves in the solar atmosphere

## VII. Non-grey, non-LTE $H^-$ models

**F. Schmitz[1], P. Ulmschneider[1], and W. Kalkofen[2]**

[1] Institut für Theoretische Astrophysik, Im Neuenheimer Feld 561, D-6900 Heidelberg, Federal Republic of Germany
[2] Harvard-Smithsonian Center for Astrophysics, 60 Garden Street, Cambridge, MA 02138, USA

Received May 29, 1984; accepted January 31, 1985

**Summary.** We study the propagation and shock formation of radiatively damped acoustic waves in the solar chromosphere under the assumption that $H^-$ is the only absorber; the opacity is non-grey. Deviations from local thermodynamic equilibrium (LTE) are permitted.

The results of numerical simulations show the depth dependence of the heating by the acoustic waves to be insensitive to the mean state of the atmosphere. After the waves have developed into shocks their energy flux decays exponentially with a constant damping length of about 1.4 times the pressure scale height, independent of initial flux and wave period.

Departures from LTE have a strong influence on the mean temperature structure in dynamical chromosphere models; this is even more pronounced in models with reduced particle density – simulating conditions in magnetic flux tubes – which show significantly increased temperatures in response to mechanical heating. When the energy dissipation of the waves is sufficiently large to dissociate most of the $H^-$ ions, a strong temperature rise is found that is reminiscent of the temperature structure in the transition zone between chromosphere and corona; the energy flux remaining in the waves then drives mass motions.

**Key words:** hydrodynamics – radiation transfer – shock waves – stars: chromospheres of – Sun (the): chromosphere of

## 1. Introduction

### 1.1. Acoustic waves and the magnetic connection

Research in recent years has shown convincingly that a heating theory based solely on acoustic waves cannot account for the observed chromospheric emission of stars (see, e.g., Linsky, 1980). Moreover, there is now wide agreement that the chromospheric emission and its variability are closely related to the magnetic field, which has a spotty distribution across the stellar surface. In particular, the solar filigree (Dunn and Zirker, 1973) and the chromospheric bright points seen in rocket observations (Brueckner, 1980; Bonnet et al., 1982; Cook et al., 1983) have been interpreted as emission signatures of narrow and intense magnetic flux tubes. This association of chromospheric emission with regions of intense magnetic flux should be taken into account in a theory of chromospheric heating.

Stein (1981) and Ulmschneider and Stein (1982) have computed generation rates of magnetohydrodynamic waves in stars with surface convection zones. They found that fast mode waves in magnetic as well as acoustic waves in non-magnetic regions are produced by quadrupole generation; but Alfvén waves and – in strong fields, acoustic-like – slow mode waves are produced by the much more efficient monopole generation. Thus Alfvén and slow mode waves are likely to be more important for chromospheric heating than are purely acoustic waves.

In regions where the magnetic field is concentrated in intense flux tubes, the Alfvén waves correspond to both transverse and torsional tube waves, and the slow mode waves correspond to longitudinal tube waves (Spruit, 1982). In these longitudinal waves the gas pressure is the principal restoring force, and in the transverse waves the magnetic field is. Therefore, the longitudinal tube waves exhibit close similarity to pure acoustic waves.

Because of the balance of gas and magnetic pressures (see, e.g., Chapman, 1981), the flux tubes spread out with increasing height and eventually form a canopy over the non-magnetic regions (Jones and Giovanelli, 1982; Anzer and Galloway, 1983). If longitudinal tube waves and purely acoustic waves propagate in a geometry defined by the shape of such a flux tube, their properties are nearly the same (cf. Herbold et al., 1985). This is due to the fact that in longitudinal tube waves the energy density of the pressure perturbation is larger by about an order of magnitude than that of the magnetic field perturbation; hence the surprising result that acoustic waves reappear as very promising for the heating of stellar chromospheres if the geometry of the magnetic field is taken into account (Ulmschneider and Stein, 1982). Chromospheric emission would therefore again be explained as a consequence of shock formation and dissipation. A continued investigation of the behavior of acoustic waves in stellar atmospheres is therefore of considerable interest.

### 1.2. The radiation

Previous work in this series of papers concentrated on the hydrodynamics of acoustic wave propagation, with simple assumptions about the radiation processes. In particular, the opacity was assumed to be grey. Using a grey LTE opacity table from Kurucz (1979), Ulmschneider et al. (1978, henceforth called Paper V) constructed theoretical models of the solar chromosphere; as seen in Fig. 1 of Paper V, a good match of the empirical chromospheric temperature rise was not obtained. Agreement with empirical models was found only when the Kurucz table was replaced by an approximate opacity formula (cf. Paper V, Fig. 2) which is a fit to the table except for reduced opacity values at low pressure. Evidently, the opacity formula implies a reduction of the efficiency with which the chromospheric gas radiates, thus simulating the effect of deviations from LTE.

*Send offprint requests to:* P. Ulmschneider

The mean chromospheric temperature structure inferred from the observations depends on the spectral feature analyzed. This point was emphasized by Praderie and Thomas (1976) and Ayres (1980) who also stressed that deviations from LTE in $H^-$ had a large effect on the energy balance in the upper photosphere and the low chromosphere. Ulmschneider and Kalkofen (1978) and Kalkofen and Ulmschneider (1979) disputed this point and estimated the mechanical heating rate at the base of the chromosphere on the assumptions that $H^-$ is the only absorber and that deviations from LTE are negligible. Subsequently Vernazza et al. (1981) showed that other absorbers make a significant contribution to the radiative cooling even at the temperature minimum, but that deviations from LTE in $H^-$ are much smaller than estimated by the previous authors. It is to be noted, however, that none of the empirical models satisfies energy conservation.

The ongoing discussion of the energy losses in the low chromosphere shows that it is necessary to study the effect of departures from LTE in a time-dependent, non-grey medium in greater detail. Such a study requires that a heating mechanism be included in the treatment because only then is it possible to solve the energy equation consistently with the mass and momentum equations. It is the aim of this paper to present such a study in the highly idealized case where $H^-$ is the only opacity source and where the detailed structure of a flux tube is ignored. The restriction of the opacity to $H^-$ is not serious since our primary interest is in the basic physics of the low chromosphere. Other absorbers, such as Mg II and Ca II as well as CO affect the details of the models (Ayres, 1981; Muchmore and Ulmschneider, 1985) but not the basic physics; these opacity sources will be included in subsequent work. The restriction of the geometry allows us to assume plane-parallel stratification of the atmosphere; the inclusion of the flux tube structure in the treatment is planned (cf. Herbold et al., 1985). In Sect. 2 we outline the approach and in Sect. 3 we present the results and give a discussion. The conclusions are summarized in Sect. 4.

## 2. The basic equations

We consider acoustic wave propagation in an atmosphere stratified in plane-parallel layers. The method of computation of such waves has been described by Ulmschneider et al. (1977), by Kalkofen and Ulmschneider (1977), and in Paper V. The energy equation is expressed in terms of the entropy $S$ (in erg $g^{-1}K^{-1}$) and the radiative cooling rate is described by the radiative damping function $D$,

$$D=\frac{dS}{dt}\bigg|_R=-\frac{\Phi_R}{\varrho T}$$

$$=\frac{4\pi}{T}\int_0^\infty[\kappa_\nu^{bf}(J_\nu-S_\nu^{bf})+\kappa_\nu^{ff}(J_\nu-B_\nu)]\,d\nu\,, \tag{1}$$

where $\Phi_R$ (erg $cm^{-3}s^{-1}$) is the net radiative cooling rate (cf. Vernazza et al., 1981), $\kappa_\nu^{bf}$ and $\kappa_\nu^{ff}$ ($cm^2g^{-1}$) are the bound-free and free-free absorption coefficients of $H^-$, $\varrho$ is the mass density, $T$ the temperature, $B_\nu$ the Planck function, and $J_\nu$ the mean monochromatic intensity. The bound-free source function for $H^-$ is given by

$$S_\nu^{bf}=\frac{2h\nu^3}{c^2}\frac{1}{b_{H^-}e^{h\nu/kT}-1}\,, \tag{2}$$

where $b_{H^-}$ is the departure coefficient of the $H^-$ ion; the other symbols have their usual meaning.

**Table 1.** Wavelength division points $\lambda_i$ (nm), frequency integration weights $W_i$ (Hz), and mean monochromatic intensities $J_{\nu_i}$ (erg $cm^{-2}s^{-1}sr^{-1}Hz^{-1}$); the latter are mostly from Vernazza et al. (1981)

| $i$ | $\lambda_i$ | $W_i$ | $J_{\nu_i}$ |
|---|---|---|---|
| 1 | $2600^+$ | 5.765 (13) | 7.97 (−6) |
| 2 | $2600^-$ | 3.620 (13) | 7.97 (−6) |
| 3 | 2400 | 1.159 (13) | 8.93 (−6) |
| 4 | 2200 | 1.198 (13) | 1.01 (−5) |
| 5 | 2000 | 1.531 (13) | 1.14 (−5) |
| 6 | 1800 | 1.758 (13) | 1.29 (−5) |
| 7 | 1642 | 1.292 (13) | 1.43 (−5) |
| 8 | 1550 | 1.147 (13) | 1.51 (−5) |
| 9 | 1450 | 1.360 (13) | 1.54 (−5) |
| 10 | 1350 | 2.116 (13) | 1.57 (−5) |
| 11 | 1200 | 2.987 (13) | 1.59 (−5) |
| 12 | 1050 | 5.123 (13) | 1.61 (−5) |
| 13 | 850 | 7.072 (13) | 1.58 (−5) |
| 14 | 700 | 9.675 (13) | 1.46 (−5) |
| 15 | 550 | 1.246 (13) | 1.16 (−5) |
| 16 | 450 | 9.099 (13) | 7.58 (−6) |
| 17 | 350 | 4.236 (13) | 2.34 (−6) |
| 18 | 200 | 7.236 (13) | 7.27 (−9) |
| 19 | 150 | 1.528 (13) | 2.49 (−11) |

We are interested in the atmospheric layers near the solar surface where the mean monochromatic intensity may be considered constant and given by the emergent intensity $J_\nu$. The values for $J_\nu$ and the frequency points are from Vernazza et al. (1981, Table 26 and Fig. 50); they are summarized in Table 1. For wavelengths longer than 1642 nm the emergent mean intensity is described by a dilute Planck function,

$$J_\nu=0.563\ B_\nu(5800\ \mathrm{K})\,. \tag{3}$$

The frequency integration is performed with $N=19$ frequency points with weighted parabolas as suggested by Kurucz (1979),

$$\int_0^\infty f(\nu)d\nu=\sum_{i=1}^N f(\lambda_i)W_i\,; \tag{4}$$

the frequency weights are also listed in Table 1.

The bound-free absorption coefficient for $H^-$ is

$$\kappa_\nu^{bf}=\frac{n_{H^-}}{\varrho}\alpha_\nu^{bf}\left(1-\frac{e^{-h\nu/kT}}{b_{H^-}}\right), \tag{5}$$

where the number density of $H^-$ ions is given by

$$n_{H^-}=b_{H^-}\frac{n_H n_e}{4}\left(\frac{h^2}{2\pi m_e kT}\right)^{3/2}e^{0.754\,\mathrm{eV}/kT}\,, \tag{6}$$

with $n_H$ the number density of neutral hydrogen atoms and $n_e$ that of electrons. The cross section for bound-free transitions of $H^-$ is (cf. Kurucz, 1970)

$$\alpha_\nu^{bf}=6.801\ 10^{-20}+(5.358\ 10^{-3}+(1.481\ 10^{13}$$
$$-(5.519\ 10^{27}-4.808\ 10^{41}/\nu)/\nu)/\nu)/\nu\,, \tag{7}$$

for $\nu>2.1110\ 10^{14}$ Hz; and

$$\alpha_\nu^{bf}=3.695\ 10^{-16}-(1.251\ 10^{-1}-1.052\ 10^{13}/\nu)/\nu\,, \tag{8}$$

for $2.1110\ 10^{14} > \nu > 1.8259\ 10^{14}$ Hz, where the lower limit is the threshold frequency for photo dissociation of $H^-$. The free-free absorption coefficient is given by

$$\kappa_\nu^{ff} = \frac{n_H}{\varrho} n_e (1.3727\ 10^{-25} + (4.3748\ 10^{-10} - 2.5993\ 10^{-7}\ T)/\nu)/\nu\,. \quad (9)$$

We note that these absorption coefficients in the form given by Kurucz (1970) are more convenient than those of Gingerich (1964) for pretabulating the opacities.

We determine the $H^-$ number density assuming that the ion is destroyed by photo dissociation,

$$H^- + \nu \leftrightarrow H + e\,, \quad (10)$$

by electron collisions,

$$H^- + e \leftrightarrow H + 2e\,, \quad (11)$$

and in associative collisional detachment by hydrogen atoms,

$$H^- + H \leftrightarrow H_2 + e\,; \quad (12)$$

the $H_2$ molecule is also formed in the reaction

$$3H \leftrightarrow H_2 + H\,. \quad (13)$$

The equations of statistical equilibrium are solved according to Gebbie and Thomas (1970) or Vernazza et al. (1973, 1981). The departure coefficient $b_{H^-}$ is given by

$$b_{H^-} = \frac{R^* + r}{R + r}\,, \quad (14)$$

where the rate coefficient ($s^{-1}$) for radiative recombination is

$$R^* = \int_{\nu_1}^{\infty} \frac{4\pi\alpha_\nu^{bf}}{h\nu} \left( \frac{2h\nu^3}{c^2} + J_\nu \right) e^{-h\nu/kT} d\nu\,, \quad (15)$$

and the coefficient for photo dissociation,

$$R = \int_{\nu_1}^{\infty} \frac{4\pi\alpha_\nu^{bf}}{h\nu} J_\nu d\nu\,. \quad (16)$$

The collisional rates are combined in the coefficient

$$r = 2\ 10^{-9} \left( \frac{n_H}{1+\delta} + \theta^{-3/2} n_e \right), \quad (17)$$

with $\theta = 5040/T$ and

$$\delta = 58\ \sqrt{\theta}\ e^{1.736\theta}\ n_e/n_H\,. \quad (18)$$

Note that Eq. (18) corrects a misprint in the corresponding equation of Vernazza et al. (1973, 1981). The departure coefficient for the $H_2$ molecule is given by

$$b_{H_2} = \frac{1 + \delta b_{H^-}}{1 + \delta}\,. \quad (19)$$

For the comparison of calculations with grey and non-grey opacities we computed grey opacity tables in LTE using Rosseland and Planck means. For the calculation of the electron density we constructed a table with $n_e$ as a function of temperature and pressure, following Kurucz (1979), neglecting departures from LTE in the principal electron donors Fe, Mg, Si, and H in order to facilitate the time-dependent solutions.

We avoided global motions of the atmosphere unrelated to the wave propagation by starting the time-dependent calculations with a radiative equilibrium atmosphere as the initial state. For the depth grid we used non-uniform spacing with intervals given by

$$\Delta x = \frac{c_S P}{N_G}\,, \quad (20)$$

where $P$ is the acoustic wave period, $c_S$ the local sound speed, and $N_G$ the number of grid points per acoustic wavelength, typically $N_G = 30$. The radiative equilibrium models were constructed by solving the equations of hydrostatic and statistical equilibrium together with the energy equation for a given radiation field, using Newton's method for calculating corrections to the state variables.

## 3. Results and discussion

### 3.1. The initial atmosphere

The initial, undisturbed atmosphere corresponds to the outer layers of a solar model in radiative equilibrium, extending from 300 km to 1000 km above the monochromatic optical depth unity at 500 nm (the bottom of this slab corresponds to $\tau_{500} = 10^{-2}$). The parameters of this model are given in Table 2; $x$ is the geometrical height and $p$ the gas pressure.

Our initial model is similar to that of Ayres (1980): his is based on the empirical model of Vernazza et al. (1976), with mean

**Table 2.** The initial radiative equilibrium model

| $x$ | $T_{RE}$ | $P$ | $n_H$ | $n_e$ | $\delta$ | $R^+$ | $b_{H^-}$ |
|---|---|---|---|---|---|---|---|
| (km) | (K) | (dyn $cm^{-2}$) | ($cm^{-3}$) | | | ($s^{-1}$) | |
| 300 | 4705 | 1.34 (4) | 1.86 (16) | 1.52 (12) | 3.14 (−2) | 1.15 (6) | 1.00 |
| 371 | 4706 | 7.04 (3) | 9.78 (15) | 8.80 (11) | 3.47 (−2) | 1.15 (6) | 1.00 |
| 442 | 4708 | 3.70 (3) | 5.13 (15) | 5.02 (11) | 3.76 (−2) | 1.15 (6) | 1.01 |
| 513 | 4713 | 1.94 (3) | 2.69 (15) | 2.84 (11) | 4.06 (−2) | 1.15 (6) | 1.01 |
| 583 | 4721 | 1.02 (3) | 1.41 (15) | 1.64 (11) | 4.43 (−2) | 1.16 (6) | 1.02 |
| 654 | 4735 | 5.37 (2) | 7.42 (14) | 9.77 (10) | 5.01 (−2) | 1.17 (6) | 1.03 |
| 726 | 4759 | 2.83 (2) | 3.89 (14) | 6.19 (10) | 5.98 (−2) | 1.20 (6) | 1.06 |
| 797 | 4794 | 1.49 (2) | 2.04 (14) | 4.22 (10) | 7.64 (−2) | 1.23 (6) | 1.09 |
| 869 | 4839 | 7.91 (1) | 1.07 (14) | 3.16 (10) | 1.07 (−1) | 1.27 (6) | 1.14 |
| 940 | 4884 | 4.20 (1) | 5.61 (13) | 2.45 (10) | 1.54 (−1) | 1.32 (6) | 1.19 |
| 1006 | 4916 | 2.38 (1) | 3.16 (13) | 1.96 (10) | 2.16 (−1) | 1.35 (6) | 1.22 |

monochromatic intensities slightly different from ours. The main differences are in the temperatures, which lead to different photo recombination rates and departure coefficients: In Ayres' model, the photo dissociation rate is $R=1.14\,10^{6}\,s^{-1}$, in ours, $R=1.10\,10^{6}\,s^{-1}$; his temperature at 300 km is 4750 K (ours, 4705 K) and at 1000 km, 5250 K (ours, 4916 K); his departure coefficient at the top of the atmosphere is $b_{H^-}=2.33$ (ours, 1.22). At 975 km the collision parameter in Ayres' model is $\delta=0.28$ [cf., Eq. (18)] resulting in a rate coefficient of $r=5.9\,10^{4}\,s^{-1}$ [cf., Eq. (17)], which agrees closely with our coefficient of $r=5.2\,10^{4}\,s^{-1}$. Thus the differences in the departure coefficient $b_{H^-}$ arise mainly from Ayres' higher temperature, which results in a photo detachment rate $R^*$ that is larger by a factor of 2.

Comparing the terms contributing to the collision coefficient [Eq. (17)] in our model we find that for $n_e \approx 10^{-4} n_H$ the second term in the parentheses is much smaller than the first. Since the uncertainty in the rate coefficient for hydrogen collisional detachment is much larger (cf. Browne and Dalgarno, 1969) we follow Jordan (1977) in neglecting electron collisional detachment. Furthermore, in both Ayres' and our model the value of $\delta$ is less than $6\,10^{-2}$ up to a height of 800 km; it is therefore neglected by the same reasoning. Thus we use the approximation

$$r=2\,10^{-9}\,n_H\,, \tag{21}$$

instead of Eq. (17).

The temperature of the radiative equilibrium atmosphere under the assumption that the gas is in LTE has the fixed value of $T_{RE}=4703$ K, independent of height. This value agrees with the kinetic temperature in non-LTE at low heights, where the departure coefficient is near unity. The increase of the kinetic temperature with height in the non-LTE case is referred to as the Cayrel effect (cf. Cayrel, 1963, 1964).

### 3.2. *Non-grey non-LTE calculation*

Figure 1 (drawn) shows the variables for a propagating acoustic wave at the time $t=1103.7$ s, measured from the initiation of the piston motion. The wave period is $P=30$ s and the acoustic flux at the lower boundary is $F_M=2.5\,10^{7}\,erg\,cm^{-2}\,s^{-1}$. This corresponds approximately to a wave flux of $F_M \approx 10^{8}\,erg\,cm^{-2}\,s^{-1}$ at $\tau_{500}=1$ (cf. Fig. 5 of Paper V). The wave is shown in the Euler frame at the instant when a weak shock is forming at the height of $x_{SH}=573$ km; the shock strength, defined as the density change in the shock transition relative to the pre-shock density, is $M_S=1.02$. At this time, 34 shocks have already been transmitted through the right boundary, and the values of the state variables averaged over a wave period have reached a steady state, indicating that the atmosphere has adjusted itself to the wave pressure and to the time-dependent heating and cooling. Note that the mean temperature, $\bar{T}$, time-averaged over one period at a fixed position in the

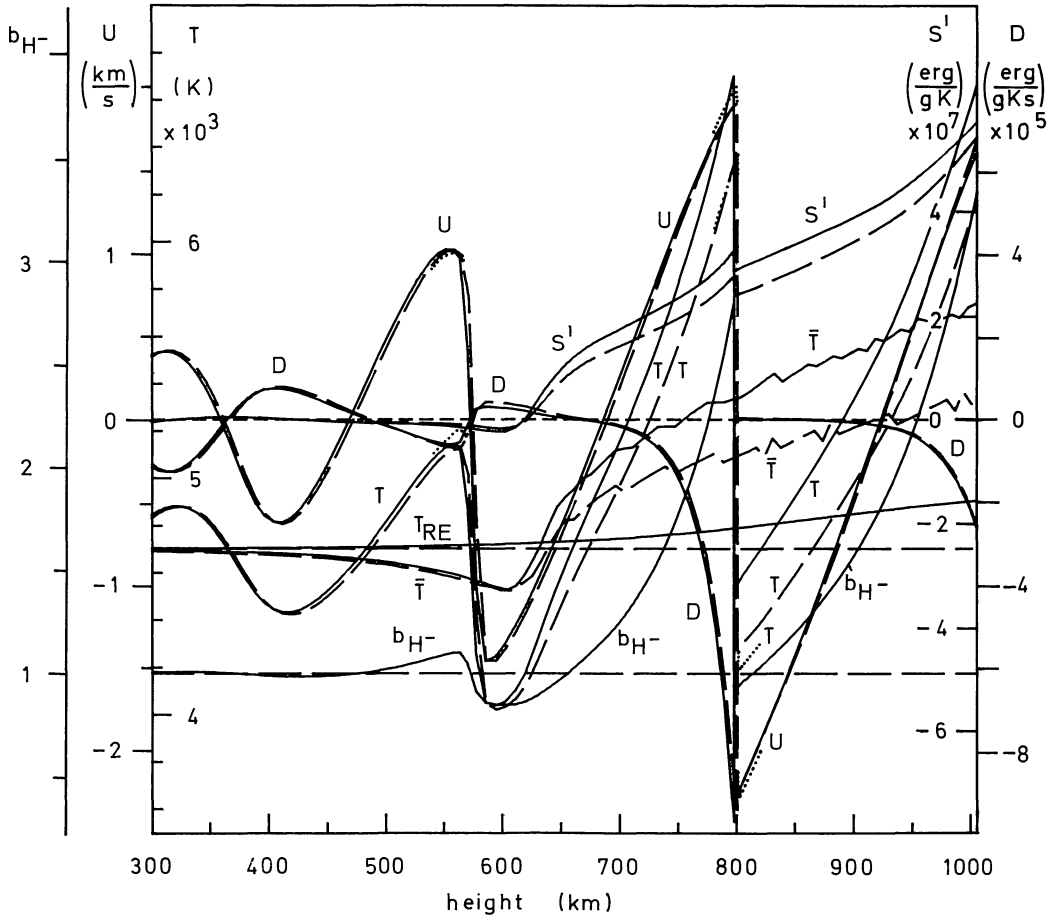


**Fig. 1.** Non-grey non-LTE *(drawn)* and LTE *(dashed)* wave calculations at the same instant of shock formation; velocity $u$, temperature $T$, mean temperature $\bar{T}$, initial radiative equilibrium temperature $T_{RE}$, radiative damping function $D=\left.\frac{dS}{dt}\right|_R$, entropy difference $S'$ from the undisturbed state, and $H^-$ departure coefficient $b_{H^-}$ as functions of Eulerian height $x$. The initial acoustic flux of the waves is $F_M=2.5\,10^{7}\,erg\,cm^{-2}\,s^{-1}$ and the period $P=30$ s; *dotted* values show the wave at an earlier time

Euler frame, is depressed below the initial radiative equilibrium temperature, $T_{RE}$; as discussed in Paper V and by Kalkofen et al. (1984), this effect is due to the non-linear response of the radiative cooling rate to waves of large amplitude. The maximal depression occurs at the temperature minimum, amounting to 195 K.

At heights greater than about $x_{SH}$, the temperature $\bar{T}$ rises rapidly above $T_{RE}$ due to heating by the shock wave. At those heights the time-averaged temperature profile $\bar{T}$ is not smooth, because of the bumpy wave profile and the coarse time grid. About one half wavelength above $x_{SH}$ the shock attains a saw-tooth profile; at the height of $x=799$ km the shock has a strength of $M_S=1.49$, which is close to the limiting shock strength of 1.46 (for $\bar{T}=5150$ K and $c_S=7.5$ km s$^{-1}$), where the limiting shock Mach number,

$$M_{SL}=1+\frac{\gamma g P}{4c_S}, \tag{22}$$

is determined from weak shock theory (cf., Ulmschneider, 1970, or Paper V).

In addition to temperature and velocity Fig. 1 also shows the radiative damping function $D$. Since the mean intensity depends only on frequency, the damping function follows the temperature oscillations with a phase lag of 180° [cf. Eq. (1)]; it decreases strongly with height except the sharply peaked high temperature region behind the shock where strong radiation losses occur due to the large temperature dependence of the emissivity. The behavior of the mean atmosphere exhibited in $\bar{T}$ is seen even more clearly in the entropy difference, $S'=S-S_0$, which describes the change in entropy of a mass element from that of the initial state. The mechanical heating of the chromosphere results in a permanent entropy gain of the atmosphere; behind the shock the entropy jump is quickly radiated away in the high temperature region.

Figure 1 also shows the departure coefficient $b_{H^-}$. Since the collisional rate coefficient $r$ is a decreasing function of height, the departure coefficient [cf. Eq. (14)] is increasingly determined by the ratio $R^*/R$ of the temperature-dependent captures and the constant radiative detachments. Thus $b_{H^-}$ oscillates in phase with the temperature, and the amplitude of the oscillation increases with height.

### 3.3. The steady state for the dynamical atmosphere

Figure 1 also shows (dotted) the wave at the earlier time $t=174.2$ s with the similar location $x=801$ km of shock formation. Except for the difference in the time-averaged temperatures as seen by comparing the temperature amplitudes of the shock, the wave has the same overall shape even though only three shocks have been transmitted through the right boundary. The strength of the shock is $M_S=1.52$, which is very close to that of the corresponding shock at the much later time. This emphasizes the fact that the amplitude and the shock dissipation of the wave are only weakly dependent on the mean state of the atmosphere.

### 3.4. Non-grey opacity in LTE; Cayrel effect

Figure 1 also shows (dashed) a wave with the gas in LTE. The shock is formed at $t=1104.1$ s, at nearly the same instant as in the non-LTE case. The two waves are very similar; the strength of the shock in LTE at $x=801$ km is $M_S=1.50$. The behavior of all variables resembles that in the non-LTE case except for the mean temperature; the maximum depression, at the temperature minimum, now has the slightly smaller value of 179 K. In the chromosphere the mean temperature is lower than in the non-LTE case; the difference between the mean chromospheric temperatures in the two cases is between two and three times the excess in the kinetic temperature of the Cayrel effect. The higher temperature in non-LTE can easily be understood from the heat balance in Eq. (1). When stimulated emissions and the free-free contribution are neglected, the equation for the radiative damping function is

$$D=\frac{4\pi}{T}\int_0^\infty \kappa_\nu^{bf*}(b_{H^-}J_\nu-B_\nu)d\nu, \tag{23}$$

where $\kappa_\nu^{bf*}$ is the opacity in LTE. It is clear that $b_{H^-}$ larger than unity acts like a higher effective temperature, thus raising the kinetic temperature in radiative equilibrium. In the time-dependent case, $b_{H^-}$ is much larger than unity in the layers above the temperature minimum for almost the entire wave period.

### 3.5. Grey LTE opacity

In order to compare our results with previous calculations of this series of papers we performed two calculations with grey opacities that differ from one another in the way the non-grey opacity is averaged over frequency. Considering again only $H^-$, we constructed grey opacity tables as suggested by Kurucz (1970) for Rosseland and Planck mean opacities as functions of temperature and pressure.

Figure 2 compares the wave calculations of the non-grey LTE (drawn) and various grey LTE cases (dashed) at the same phase of shock formation and number of shocks transmitted. The grey models differ from the non-grey model only slightly in the value of the mean chromospheric temperature. This close agreement is attributable to the smooth frequency dependence of the $H^-$ opacity. We have also repeated a grey LTE calculation using the Kurucz (1979) opacity table (cf. Fig. 2), which includes many absorbers in addition to $H^-$. Their effect is to increase the efficiency with which the chromospheric gas radiates and thus reduces the chromospheric temperature rise, in agreement with the results of Paper V. Note that the wave amplitude and the shock strength are hardly affected by the value of the opacity and the efficiency of the emission (cf. Sect. 3.9, below).

### 3.6. Waves with higher energy

At the top of the atmosphere ($x=1000$ km), the mean temperature of 5540 K in Fig. 1 is lower than that of the empirical model (5755 K in model C of Vernazza et al., 1981). It is interesting to ask whether an increase in the wave amplitude might increase the temperature. Figure 3 shows the result of a non-grey non-LTE calculation for a 30 s wave with a tenfold increase in the energy flux of the wave, i.e., $F_M=2.5\ 10^8$ erg cm$^{-2}$ s$^{-1}$. The comparison with Fig. 1 shows that the mean chromospheric temperature is hardly affected by this larger flux, and the shock strength, $M_S=1.64$ at $x=615$ km and $M_S=1.59$ at 860 km, is not very different from that of the shocks in Fig. 1. Thus the wave dissipation at chromospheric heights is not much changed, but below 700 km the models are quite different. Because of the large amplitude and the associated non-linear distortion of the wave profile, shocks form lower in the atmosphere at $x_{SH}=394$ km (cf. Ulmschneider et al., 1977). Below this height the higher flux produces a larger temperature depression, which reaches 390 K at the temperature minimum. Shock dissipation for heights larger than $x_{SH}$ raises the temperature by about the same amount, leading to large radiation losses. At about 700 km most of the higher energy flux of this wave has been dissipated, resulting in an energy balance and structure of the atmosphere similar to that shown in Fig. 1 for the weaker wave.

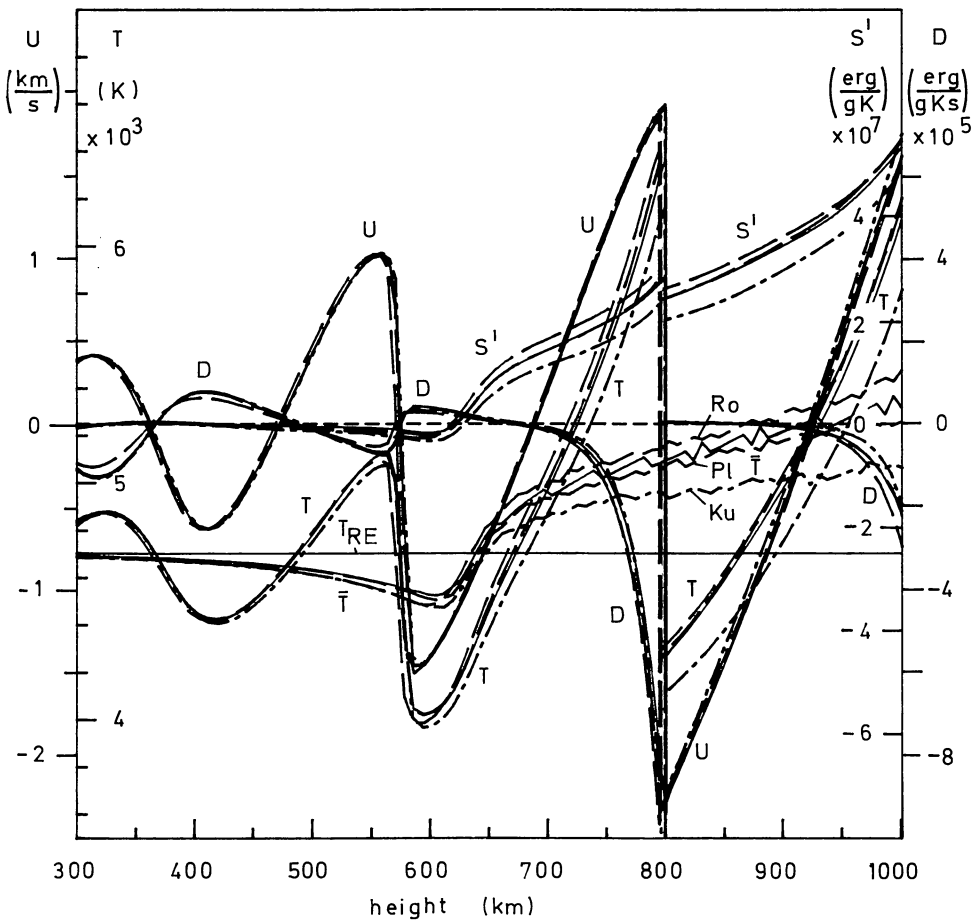


**Fig. 2.** Comparison of waves for non-grey LTE opacity *(drawn)* of Fig. 1 with various grey LTE cases at the same instant of shock formation [Ro = Rosseland mean, Pl = Planck mean, Ku = Kurucz (1979) opacity table]

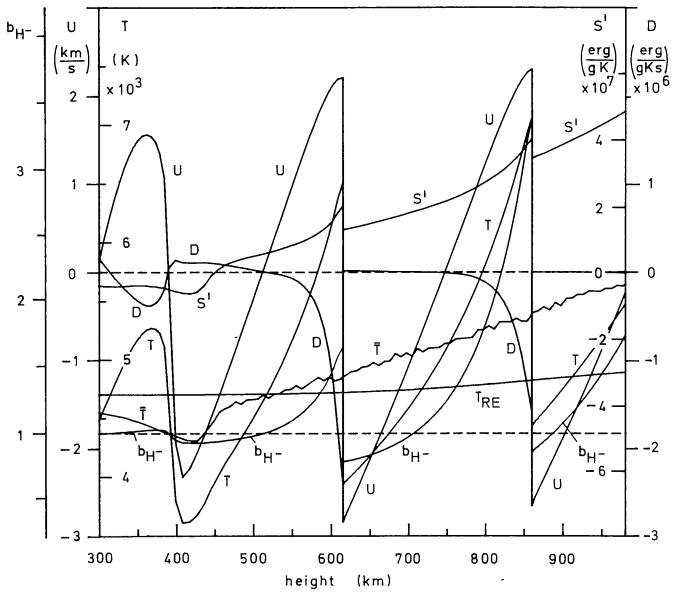


**Fig. 3.** Same as Fig. 1 (non-LTE), except for increased mechanical flux, $F_M = 2.5\,10^8$ erg cm$^{-2}$ s$^{-1}$

### *3.7. Waves in atmospheres with lower density*

Observations suggest that the mechanical energy that heats the low chromosphere travels mainly in magnetic flux tubes; this is in agreement with the study of the solar temperature structure near the temperature minimum by Kalkofen et al. (1984). In these flux tubes the gas density is much lower than in the surrounding atmosphere on account of the contribution of the magnetic field to the pressure balance. A detailed computation of the wave transport and heating in the tubes (cf. Herbold et al., 1984) is beyond the scope of this investigation. It is nevertheless interesting to study the response of an atmosphere of lower density to mechanical heating. Figure 4 shows the results of a non-grey non-LTE calculation for a 30 s wave with a flux of $F_M = 2.5\,10^7$ erg cm$^{-2}$ s$^{-1}$ in an atmosphere in which the gas density is reduced by a factor of ten.

The comparison of Figs. 3 and 4 shows that the decreased density leads to the same initial wave amplitude as in the high-flux case. Other similarities are the low height of shock formation of $x_{SH} = 387$ km, the nearly identical shock strengths ($M_S = 1.63$ and $M_S = 1.56$) and shock positions (621 and 874 km). The small differences in shock position are due mainly to the larger sound speed, caused by the higher mean kinetic temperature, $\bar{T}$, which is increased by the astounding amount of 500 to 1000 K. As follows from the much larger value of the departure coefficient $b_{H^-}$, this mean temperature increase is caused primarily by non-LTE effects, due to the decreased radiative efficiency of the atmosphere. These non-LTE effects are the result of the reduced collision rates in the low-density atmosphere. Note that the density is so low that the radiative equilibrium temperature $T_{RE}$ attains nearly the maximum value of the Cayrel effect. Note also that the difference in the values of the mean temperatures in Figs. 3 and 4 is much larger than that of the radiative equilibrium temperatures. The low density calculation thus shows that flux tube models can lead to

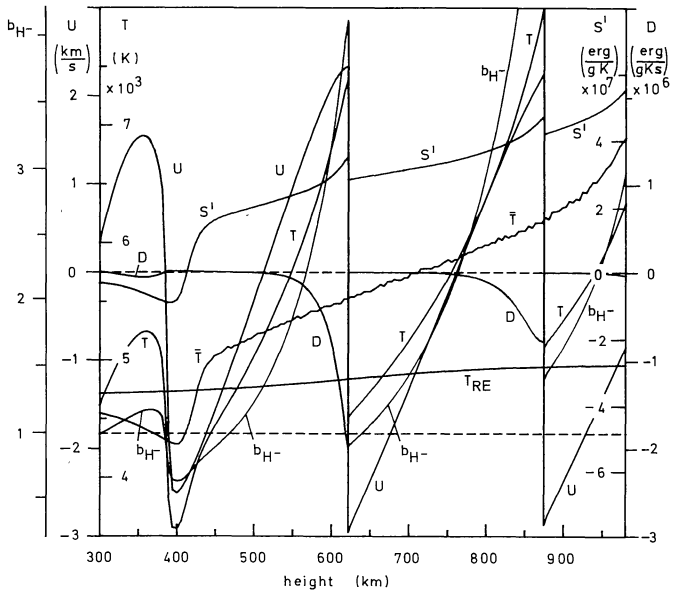


**Fig. 4.** Same as Fig. 1 (non-LTE), except for reduction of ambient density by a factor of ten

much higher kinetic temperatures than those of mean models of the chromosphere.

### 3.8. *Waves with longer periods*

Another method of raising the chromospheric temperature is by increasing the wave period. As shown by Ulmschneider and Kalkofen (1977), radiation damping in the photosphere decreases with increasing wave period, and shocks form at greater heights and are stronger. Increasing the wave period thus effectively increases the wave energy reaching the chromosphere. Figure 5 shows non-grey non-LTE solutions with a period of 60 s and an energy flux of $F_M = 2.5\,10^7\,\mathrm{erg\,cm^{-2}\,s^{-1}}$ at time $t = 1100$ s at the moment of shock formation, with strength $M_S = 1.02$ and at a height of

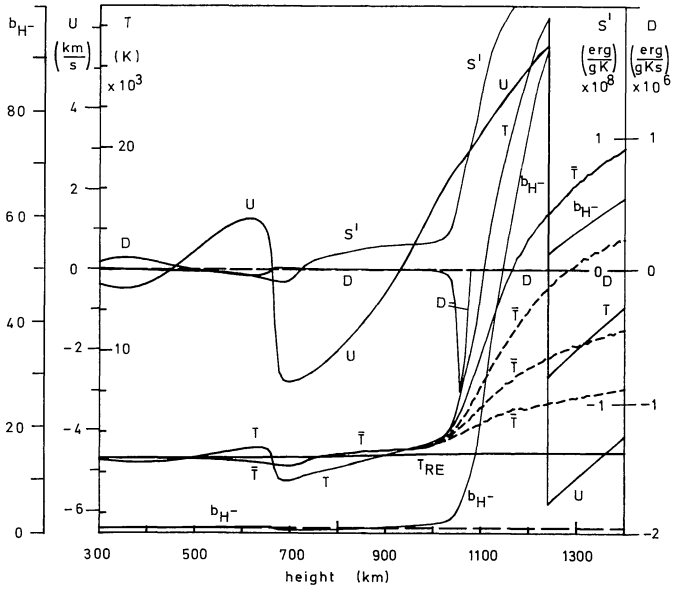


**Fig. 5.** Same as Fig. 1 (non-LTE), except for $P = 60$ s at time $t = 1100$ s. Time-averaged mean temperatures, $\bar{T}$, *(dashed)* at earlier times (from bottom to top), $t = 320$ s, 501 s, 800 s; at $t = 0$, $\bar{T} = T_{RE}$

$x_{SH} = 664$ km; 16 shocks have been transmitted at the right boundary. The shock at $x = 1240$ km has a strength of $M_S = 1.77$. This value is approximately what one expects [cf. Eq. (22)] for the limiting shock strength when the period is doubled.

After they are fully developed the sawtooth shocks in the chromosphere are much stronger and dissipate more energy. At heights below 1000 km (cf. Fig. 5) the temperature behind the shock is only moderately high and most of the dissipated energy is radiated away immediately behind the shock front. (The behavior of the entropy is similar to that shown in Fig. 1.) The time interval between arrivals of shocks is increased, giving the atmosphere more time to cool. The result of the opposing effects of stronger dissipation and longer wave period is for the mean temperature to rise only very slowly. The comparison with Fig. 1 shows that, below 1000 km, $\bar{T}$ increases even more slowly with height than in the case of the 30 s wave.

Above a height of 1000 km another effect becomes important. Since the shock is now fully developed and fairly strong, the temperature jump between the front and the back of the shock is about $10^4$ K. The temperature behind the shock has become so high that $H^-$ is destroyed and ceases to cool the atmosphere. This is seen in Fig. 5 where the radiative damping function $D$ has a sharply pronounced minimum far behind the shock front; this is different from the case of weaker shocks, where the minimum of the function $D$, i.e., the strongest emission, occurs immediately behind the shock (cf. Fig. 1). The destruction of $H^-$ behind the shock thus has the consequence of inhibiting the gas from radiating away the mechanical energy quickly enough before the next shock arrives, hence the mean temperature increases. This is shown in Fig. 5, where the $\bar{T}$ distributions for several intermediate times are given. Since the rising mean temperature increases both the preshock and the postshock temperatures this process amplifies itself and leads to a transition layer-like structure, analogous to the solar transition zone between chromosphere and corona.

The situation described here is artificial because of the neglect of such important opacity sources as the Ca II, Mg II, and Lyman lines that would provide cooling at heights where the $H^-$ density has become too low to be effective. Nevertheless, the present calculation demonstrates what happens when an important coolant disappears. It shows what may occur when Lyman-$\alpha$ becomes unimportant because of the ionization of hydrogen.

When the height range in the models extends far enough a rapid temperature rise (henceforth called "transition layer") forms in all (LTE and non-LTE) cases. For the given initial acoustic energy flux of $F_M = 2.5\,10^7\,\mathrm{erg\,cm^{-2}\,s^{-1}}$ the "transition layer" forms at a height increasing with decreasing wave period (in non-LTE: for $P = 60$ s near $x = 1100$ km, for $P = 45$ s near $x = 1200$ km, and for $P = 30$ s near $x = 1400$ km; in LTE: for $P = 60$ s near $x = 1200$ km and for $P = 45$ s near $x = 1300$ km). For the gas in LTE, the higher radiative efficiency causes the "transition layer" to be formed at a greater height than in non-LTE.

The enormous reduction in the efficiency to cool the atmosphere in the presence of strongly dissipating shocks has another interesting consequence. Since energy balance is strictly enforced, only mass motions remain as an energy sink when cooling by radiation is eliminated (these mass motions are not at all obvious in the Eulerian frame, which was obtained from the Lagrangian frame by interpolating back to the fixed Eulerian mesh). A mass flux can be estimated from the speed of the topmost Lagrange point, i.e., from the mass element that was initially at the height $x = 1440$ km; after $t = 1100$ s, this element was displaced to $x = 3110$ km. With an average speed of displacement of $1.7\ \mathrm{km\,s^{-1}}$ and a density decrease from $1.7\,10^{-12}$ to $1.5\,10^{-13}\,\mathrm{g\,cm^{-3}}$ an

approximate transient mass flux of $\varrho v = 2.6\,10^{-8}\,\mathrm{g\,cm^{-2}s^{-1}}$ is found, corresponding to about $10^3$ times the solar mass loss rate.

### 3.9. *Wave flux and mechanical heating rate*

Another interesting insight into the basic physics of acoustic wave propagation in a stellar atmosphere can be gained by studying the behavior of the acoustic wave flux, $F_M$, and the mechanical heating rate, $\Phi_M$. Figure 6 shows the development of the time-averaged quantities as functions of height. At low height, both the flux and the mechanical heating rate,

$$\Phi_M \equiv \frac{dF_M}{dx}, \tag{24}$$

decrease rapidly in all calculations, due to radiation damping. For sufficiently low initial flux $F_M$ the waves reach a nearly adiabatic phase at the end of which shocks form, owing to non-linear effects brought on by the growing wave amplitude. The shocks gain rapidly in strength (cf. Fig. 1). After reaching a fully developed sawtooth shape the mechanical flux decays logarithmically with height (Fig. 6),

$$\frac{dF_M}{dx} = -\frac{F_M}{L}, \tag{25}$$

where the damping length $L$ is nearly the same constant in all cases. In the present work we find $L \approx 175$ km which is similar to the value of $L = 172$ km obtained in Paper V. Note that $L$ is comparable to the pressure scale height ($H = 129$ km for $T = 5500$ K). This damping behavior is similar to that of weak shocks of limiting strength in isothermal atmospheres, where $L$ is equal to the scale height (cf. Paper V).

The mechanical heating rate $\Phi_M$ behaves similarly,

$$\frac{d\Phi_M}{dx} = -\frac{\Phi_M}{L}, \tag{26}$$

as can be seen from Fig. 6, or by differentiating Eq. (25) with respect to height, using Eq. (24). The interesting point is that for all cases, whether LTE or non-LTE, the mechanical heating rates for different initial fluxes and wave periods cannot be distinguished on the basis of their depth dependence. This shows that the dissipation of fully developed shocks is insensitive to deviations from LTE or to the opacity sources. It also demonstrates that the mean state of the atmosphere must depend primarily on the rate of radiative cooling. In the steady state, the mechanical heating rate $\Phi_M$ at a given height is a fixed quantity, which must be balanced by the net radiative cooling rate $\Phi_R$. If large departures from LTE keep the emission efficiency low, the mean chromospheric temperature must be high in order to satisfy the condition,

$$\Phi_M = \Phi_R\,. \tag{27}$$

On the other hand, if the emission efficiency is high, as it is in LTE, the mean chromospheric temperature will be low. Thus the chromospheric temperature rise is strongly enhanced by large departures from LTE.

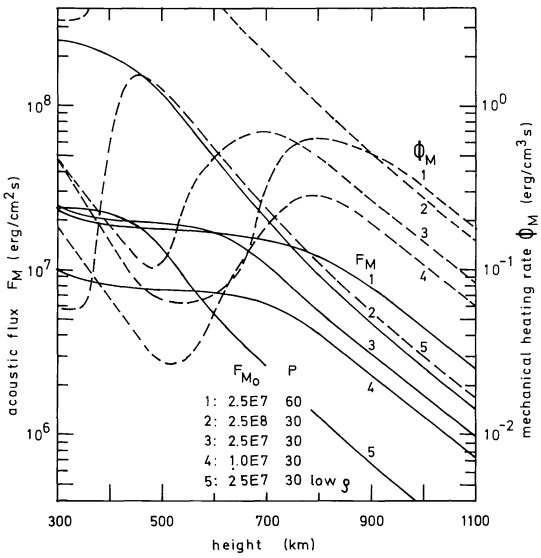


**Fig. 6.** Mechanical fluxes $F_M$ and heating rates $\Phi_M$

### 3.10. *Discussion of previous work*

Over the past ten years a lively discussion was held in the literature (Praderie and Thomas, 1972, 1976; Ulmschneider, 1974; Ulmschneider and Kalkofen, 1978; Cram, 1978; Kalkofen and Ulmschneider, 1979; Ayres, 1980; Vernazza et al., 1981) about the proper way to estimate the radiative losses in $H^-$ from empirical model atmospheres. This discussion focussed mainly on the use of the energy Eq. (1). From the present work (cf. Fig. 2) it is clear that, as far as $H^-$ is concerned, the choice of grey or non-grey opacity does not make much difference. Hence a formula [cf. Eq. (1)] of the type

$$\Phi_R = 4\pi\varrho\bar{\kappa}(J - S) \tag{28}$$

with the mean opacity, $\bar{\kappa}$, used by Ulmschneider (1974), is adequate; and the question of a factor of two to account for outward and inward radiation is settled in favor of Ulmschneider's result, as has been pointed out again by Cram (1978).

Praderie and Thomas criticized the use of Eq. (28) by Ulmschneider (1974) for deducing the net radiative cooling rate $\Phi_R$ from empirical models. Such models are constructed to satisfy observational constraints and do not attempt to satisfy the energy equation. To assume that the gas at the temperature minimum is in radiative equilibrium with $H^-$ as the *only* opacity source can indeed be quite misleading. Hence the use of the equation

$$J = B(T_0), \tag{29}$$

where $T_0$ is the minimum temperature, is inappropriate, in particular since $H^-$ is a source of heating of the gas (Vernazza et al., 1981) and the CO molecule, for example, is a coolant (Ayres, 1980). Furthermore, the observations do not suggest a unique static temperature at the temperature minimum even in the quiet sun, making it appear likely that the solar atmosphere is not in static equilibrium (Kalkofen, 1981; Kalkofen et al., 1984).

The present calculations should be taken as a warning that the reasoning based on static models may be in error. In the temperature minimum region, non-linear effects due to mechanical waves of large amplitude can lead to a significantly depressed temperature at which the static energy equation will not be satisfied. In addition, the high temperature peaks of these waves are weighted preferentially in lines formed in the ultra-violet, leading to high values for the inferred temperatures in models based on lines. Thus, on the basis of the dynamical model of the solar atmosphere, a unique temperature distribution for a static model of the temperature minimum region is not expected. This is true also for the chromosphere, where the large temperature variations due to shocks have emission characteristics that are quite different from those of a smooth static temperature distribution.

While deviations from LTE in $H^-$ may not be very important at the temperature minimum, they are crucial for the temperature structure of the chromosphere, as had been emphasized by Praderie and Thomas (1976) in criticizing the approach taken by Ulmschneider (1974). This point is confirmed by the calculations reported here, which demonstrate that a temperature rise like that of the empirical models is found only if deviations from LTE are taken into account.

## 4. Conclusions

We have constructed non-grey non-LTE models of the solar atmosphere with acoustic heating and with $H^-$ as the only opacity source, solving the time-dependent equations of mass, momentum, and energy conservation together with the statistical rate equations. Our calculations reveal several general properties of radiatively damped acoustic waves in the solar atmosphere:

1) The shape of the wave profile, shock strength, acoustic flux, and shock dissipation rate depend very little on the mean state of the atmosphere through which a wave propagates (cf. Figs. 1 and 6). For a given initial wave flux $F_M$ and period $P$, the mechanical heating rate $\Phi_M$ is found to be a specific function of height independent of assumptions about the (LTE or non-LTE) state of the gas (Fig. 6).

2) The LTE wave calculations with grey and non-grey opacity give practically the same result (Fig. 2). This is true regardless of the frequency-averaging procedure for the opacity. We attribute this to the smooth frequency dependence of the $H^-$ opacity.

3) The time-averaged mean temperature of non-LTE models is always significantly higher than that of LTE models. This is especially true for atmospheres with reduced density, which are relevant for models of magnetic flux tubes. The mean state of the atmosphere is controlled by the radiative emission rate. Because of the low mean intensity at the stellar surface, upper levels tend to be underpopulated relative to lower levels, leading to a reduction in the radiative cooling rate. Thus, for a given temperature, a gas with deviations from LTE usually emits less than a gas in LTE. Since energy conservation forces the net radiative cooling rate $\Phi_R$ to be equal to the mechanical heating rate $\Phi_M$, non-LTE models have higher kinetic temperatures than LTE models.

4) The nearly total dissociation of $H^-$ leads to the formation of a transition layer-like rapid temperature rise. Since radiative cooling is then unable to balance mechanical heating, transient mass motions with $\varrho v$ corresponding to $10^3$ times the solar mass loss rate are initiated. All our models (LTE and non-LTE) developed transition layer-like rapid temperature rises if the atmospheric slab extended far enough (Fig. 5).

5) Additional emitters like the Ca II, Mg II, and Lyman lines would delay the formation of these transition layer-like structures. It is likely that the destruction of the dominant Ly $\alpha$ emitter due to hydrogen ionization is the cause of the observed transition layer.

6) There is a tendency for waves with shorter period (Fig. 1) to heat preferentially the low chromosphere and those with longer period (Fig. 5) to heat the upper chromosphere. For long period waves, more energy remains for driving mass motions.

*Acknowledgements.* We gratefully acknowledge the generous support of the Deutsche Forschungsgemeinschaft (SFB 132), the National Science Foundation (grant AST 83-03252), and NASA (grant NAGW-253).

## References

Anzer, U., Galloway, D.J.: 1983, in *Solar and Stellar Magnetic Fields*, IAU *Symp.* **102**, ed. J.O. Stenflo, p. 339
Ayres, T.R.: 1980, *Solar Phys.* **68**, 125
Ayres, T.R.: 1981, *Astrophys. J.* **244**, 1064
Bonnet, R.M., Bruner, M., Acton, L.W., Brown, W.A., Decaudin, M., Foing, B.: 1982, *Astron. Astrophys.* **111**, 125
Brueckner, G.E.: 1980, *Highlights of Astronomy* **5**, 557
Browne, J.E., Dalgarno, A.: 1969: *J. Phys. B* **2**, 885
Cayrel, R.: 1963, *Compt. Rend. Acad. Sci. Paris* **257**, 3309
Cayrel, R.: 1964, *Smithsonian Astrophys. Obs. Spec. Rept.* **167**, 169
Chapman, G.A.: 1981, Solar Active Regions, ed. F.Q. Orrall, Colorado Assoc. Univ. Press, Boulder, p. 43
Cook, J.W., Brueckner, G.E., Bartoe, J.-D., F.: 1983, *Astrophys. J.* **270**, L89
Cram, L.E.: 1978, *Astron. Astrophys.* **67**, 301
Dunn, R.B., Zirker, J.B.: 1973, *Solar Phys.* **33**, 281
Gebbie, K.B., Thomas, R.N.: 1970, *Astrophys. J.* **161**, 229
Gingerich, O.: 1964, *Smithsonian Astrophys. Obs. Spec. Rept.* **167**, 17
Herbold, G., Ulmschneider, P., Spruit, H.C., Rosner, R.: 1985, *Astron. Astrophys.* **145**, 157
Jones, H.P., Giovanelli, R.G.: 1982, *Solar Phys.* **79**, 247
Jordan, S.D.: 1977, *Solar Phys.* **51**, 51
Kalkofen, W.: 1981, *Smithsonian Astrophys. Obs. Spec. Rept.* **392**, 59
Kalkofen, W., Ulmschneider, P.: 1977, *Astron. Astrophys.* **57**, 193
Kalkofen, W., Ulmschneider, P.: 1979, *Astrophys. J.* **227**, 655
Kalkofen, W., Ulmschneider, P., Schmitz, F.: 1984, *Astrophys. J.* **287**, 952
Kurucz, R.: 1970, *Smithsonian Astrophys. Obs. Spec. Rept.* **309**
Kurucz, R.: 1979, *Astrophys. J. Suppl.* **40**, 1
Linsky, J.L.: 1980, *Ann. Rev. Astron. Astrophys.* **18**, 439
Muchmore, D., Ulmschneider, P.: 1985, *Astron. Astrophys.* **142**, 393
Praderie, F., Thomas, R.N.: 1972, *Astrophys. J.* **172**, 485
Praderie, F., Thomas, R.N.: 1976, *Solar Phys.* **50**, 333
Spruit, H.C.: 1982, *Solar Phys.* **75**, 3
Stein, R.F.: 1981, *Astrophys. J.* **246**, 966
Ulmschneider, P.: 1970, *Solar Phys.* **12**, 403
Ulmschneider, P.: 1974, *Solar Phys.* **39**, 327
Ulmschneider, P., Kalkofen, W.: 1977, *Astron. Astrophys.* **57**, 199
Ulmschneider, P., Kalkofen, W., Nowak, T., Bohn, U.: 1977, *Astron. Astrophys.* **54**, 61
Ulmschneider, P., Kalkofen, W.: 1978, *Astron. Astrophys.* **69**, 407
Ulmschneider, P., Schmitz, F., Kalkofen, W., Bohn, H.U.: 1978, *Astron. Astrophys.* **70**, 487 (Paper V)
Ulmschneider, P., Stein, R.F.: 1982, *Astron. Astrophys.* **106**, 9
Vernazza, J.E., Avrett, E.H., Loeser, R.: 1973, *Astrophys. J.* **184**, 605
Vernazza, J.E., Avrett, E.H., Loeser, R.: 1976, *Astrophys. J. Suppl.* **30**, 1
Vernazza, J.E., Avrett, E.H., Loeser, R.: 1981, *Astrophys. J. Suppl.* **45**, 635